Pergamon

Geochimica et Cosmochimica Acta, Vol. 66, No. 12, pp. 2123–2138, 2002

0016-7037/02 $22.00 + .00

PII S0016-7037(02)00827-X

Kinetics of the reaction $MgO + Al_2O_3 \rightarrow MgAl_2O_4$ and Al-Mg interdiffusion in spinel at 1200 to 2000°C and 1.0 to 4.0 GPa

E. Bruce Watson* and Jonathan D. Price

Department of Earth and Environmental Sciences, Rensselaer Polytechnic Institute, Troy, NY 12180, USA

(*Received May* 31, 2001; *accepted in revised form December* 31, 2001)

Abstract—The rate of spinel ($MgAl_2O_4$) growth at the interface between MgO and Al_2O_3 was investigated systematically at temperatures of 1200° to ~2000°C and pressures between 1.0 and 4.0 GPa with a solid-media, piston-cylinder apparatus. As reported in previous 1-atm studies, the thickness (ΔX) of the spinel layer increases linearly with the square root of time for experiments differing only in duration, irrespective of pressure–temperature (P-T) conditions. The reaction rate constant ($k = \Delta X^2/2t$) is log-linear in 1/T and also in pressure. The apparent activation energy of 410 kJ/mol is independent of pressure; the apparent activation volume increases systematically with increasing temperature. Electron microprobe traverses across the spinel layer reveal a significant Al excess and charge-compensating Mg deficit near the spinel/corundum interface. This nonstoichiometry is promoted by high temperatures (>1500°C), suppressed by high pressures and varies linearly across the spinel to a near-stoichiometric composition at the interface with periclase. The Al and Mg composition gradients can be used to extract interdiffusion coefficients for Al ↔ Mg exchange through the spinel, which are described by

$$\tilde{D} = 2.5 \times 10^{-6} \exp(-28200/T) \quad m^2 s$$

These diffusivities differ substantially from the reaction rate constant *k*, reflecting the fact that *k* is a combination of the diffusivity and the reaction potential as indicated by the difference in spinel composition across the spinel layer (i.e., coexisting with corundum vs. coexisting with periclase). A simple model can be used to separate the two effects and show that the reaction potential (i.e., the MgO-Al_2O_3 phase diagram) is sensitive to changes in both temperature and pressure, whereas the governing diffusivity depends only on temperature.

1. INTRODUCTION

The technological importance of MgO (periclase) and Al_2O_3 (corundum) in refractory ceramics has prompted numerous studies of the kinetics of the reaction between these two oxides at temperatures of 1200 to 1900°C and near-atmospheric pressure (e.g., Carter, 1961; Rossi and Fulrath, 1963; Yamaguchi and Tokuda, 1967; Whitney and Stubican, 1971a,b; MacKenzie and Ryan, 1981; Li et al., 1992; Zhang et al., 1996; Ting and Lu, 1999). On the whole, these studies are in reasonably good agreement as to the general rate and temperature dependence of the reaction, but the mechanism remains controversial. Most researchers report a parabolic time dependence of spinel growth between contacting periclase and corundum, indicating diffusion control. The details of the diffusion process and the nature the gradients driving diffusion are less clear. Control of spinel growth is attributed variously to grain-boundary diffusion (e.g., MacKenzie and Ryan, 1981) or lattice diffusion of Mg, Al, or both in spinel (e.g., Carter, 1961; Zhang et al., 1996), or to diffusion in the reactant oxides (e.g., Navias, 1961). Some researchers concluded that crystallographic orientation affects the reaction kinetics (e.g., Whitney and Stubican, 1971a,b), whereas others see no effects of lattice orientation. Disagreement also surrounds the nature of the governing phase relations, in particular the composition of spinel coexisting with periclase or corundum as a function of temperature. Diffusion of oxygen in the product spinel has generally been regarded as unimportant to the overall kinetics of the reaction (but see Ting and Lu, 1999).

The reaction between MgO and Al_2O_3 is of significant interest in geochemistry and petrology for at least two reasons. First, the simple, spinel-producing reaction has not been studied at elevated pressures, so the MgO-Al_2O_3 system provides an opportunity to investigate the rate and mechanism of a simple, two-oxide reaction as a function of the two variables (temperature [T] and pressure [P]) important in the Earth. The results of such a study could aid in the understanding of reactions between more complex oxides in natural rocks, of which there are numerous examples in the literature—accompanied, in some cases, by general theoretical treatments (e.g., Joesten, 1977; Johnson and Carlson, 1990; Carlson and Johnson, 1991; Ashworth and Sheplev, 1997). In its examination of a very simple system, the present investigation might be seen as a step backward. Viewed in a more positive way, however, the study provides a comprehensive set of basic data leading to a simple, testable model. The model provides information on actual diffusion mechanisms and interface motions that is not readily recovered from studies of complex natural systems.

A second reason for interest in the spinel-producing reaction, among experimental geoscientists specifically, is that MgO and Al_2O_3 are widely used refractory ceramics in high P-T systems. They are available in both dense and machinable forms suitable for use as filler pieces and spacers in piston-cylinder and multianvil pressure assemblies. Data pertaining to the rate of spinel growth at MgO/Al_2O_3 interfaces as a function of tem-

*Author to whom correspondence should be addressed (watsoe@rpi.edu).

perature and pressure are therefore potentially useful for mapping P-T-t conditions within these assemblies. The focus of this article is primarily on the kinetics and thermodynamics of the interaction between MgO and Al_2O_3, including the rate of spinel growth; the mechanism of the diffusion processes involved; and the nature and consequences of the phase relations. Application to temperature mapping and pressure calibration in solid-media pressure assemblies has been dealt with elsewhere (Watson et al., 2002).

2. EXPERIMENTAL MATERIALS AND METHODS

All experiments were conducted in an end-loaded, Boyd and England (1960)–type piston-cylinder apparatus with either 13- or 19-mm diameter pressure assemblies consisting of an NaCl outer sleeve, a glass thermal insulator sleeve (Pyrex or SiO_2, depending on the P-T conditions of the individual experiment), a tubular graphite heater, and a combination of MgO and Al_2O_3 inner filler pieces in various configurations (Fig. 1). The ordinary filler pieces served as the reacting phases in many experiments, but several configurations and other forms of MgO and Al_2O_3 were also used. Each experiment included dense polycrystalline Al_2O_3 as the thermocouple insulator, which was in contact with dense polycrystalline MgO along its entire length—that is, the upper half of the pressure cell (Fig. 1). The thermocouple insulator, purchased from Vesuvius McDanel, is 99.8% Al_2O_3 and has a preexperiment grain size of 5 to 30 μm. The dense polycrystalline MgO filler pieces, purchased from Saint-Gobain/Norton, are 99.7% MgO (SiO_2 and Al_2O_3 are the main impurities) and have an initial grain size of ~1 to 100 μm. Single-crystal MgO and Al_2O_3 were incorporated in some of the experiments in the form of diffusion couples and "sandwiches" of three or more layers. Optically clear MgO crystals used for this purpose were supplied by Cerac Inc. and have a typical purity of 99.95%. These were cleaved to obtain smooth surfaces for mating with Al_2O_3. Single-crystal corundum of 99.97% purity was purchased from Alfa Aesar as 1-cm square slabs (sold as "substrates") oriented perpendicular or parallel to the *c* crystallographic axis. These slabs were of 0.5 or 1 mm nominal thickness, prepolished commercially to a surface that is featureless under the scanning electron microscope. They were cut into usable sizes with a low-speed diamond saw.

In a few experiments, 4-μm-thick Pt foil was inserted along a portion of the contact between MgO and Al_2O_3 as an inert reference marker that was intended to facilitate quantification of component fluxes during the experiments. Quantitative treatment was ultimately successful, but not because of the presence of the Pt marker. The various single-crystal and polycrystal interdiffusion couple arrangements are illustrated in Figure 2.

A single $W_{97}Re_3/W_{75}Re_{25}$ thermocouple was used in all experiments, with no correction for the recognized pressure effect on the emf (Mao and Bell, 1971). A change in thermocouple wire lots was made after run number 51; this is noteworthy because the calibration of the new wire spools provided by the supplier (Englehard) was significantly different from that used in most of the other runs, especially at temperatures exceeding ~1500°C. A correction was therefore applied to the nominal temperatures of the last few runs (runs 52 to 54) to make them consistent with the rest of the experiments (this is the why the temperatures of these runs depart from the normal 100-degree interval; Table 1). The sample pressure was taken as that given directly by the oil pressure acting on the hydraulic ram driving the carbide piston. Previous calibrations in our laboratory that were based on the melting curves of Au and NaCl have shown that our cell design is essentially "frictionless" in the 1.0- to 1.5-GPa range, with apparent pressures within ~20 MPa of actual values. The experiment run-up involved cold pressurization to a value exceeding the desired run pressure by 10 to 20%, allowing for "settling" (relaxation) of the assembly on heating. The final desired run pressure can be closely approached by means of this technique, necessitating only minor (upward) pressure adjustments later in the run in most cases. This run-up procedure could be described as "hot piston-in"; however, such a characterization is probably too simplistic because runs of extended duration require repeated minor upward adjustments in apparent pressure over the first ~2 to ~24 h, depending on temperature.

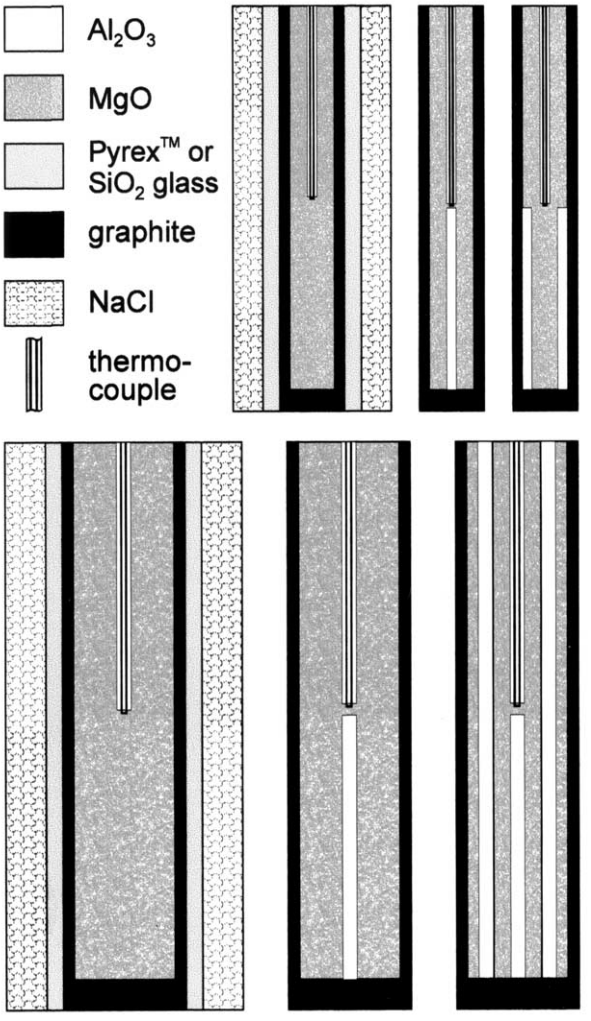

Fig. 1. Scale drawings representing axial sections of the piston-cylinder assemblies used in this study that show various configurations of MgO and Al_2O_3 filler pieces (top row, 13-mm diameter; bottom row, 19-mm diameter). The NaCl outer sleeve is depicted only in the first schematic of each row. The outer Al_2O_3 pieces in the rightmost schematics are tubular in shape and coaxial with the thermocouple insulator. See text for details.

The experimental conditions covered in this study range from 1200° to ~2000°C and 1.0 to 4.0 GPa. Only a few runs were made above the range of routine piston-cylinder operation (i.e., pressures above ~3 GPa and temperatures above ~1700°C). Below 1200°C, the rate of spinel formation was too slow to measure accurately in experiments of reasonable duration. A summary of experiment conditions and durations is listed in Table 1.

Experiments were terminated by thermal quenching (~10 s for 13-mm assemblies; 20 to 30 s for 19-mm assemblies) followed by depressurization and recovery of the assembly from the pressure vessel. The NaCl pressure medium and the glass insulator sleeve were removed and the remaining parts of the cell impregnated with epoxy to limit disaggregation along decompression cracks (a procedure that was not always completely successful). The assembly was then sawn in two vertically, close to the cylinder axis. The larger piece was impregnated a second time and cast in epoxy, then ground with a diamond whetstone to expose a planar section along the assembly axis. The ground surface was prepared for analysis by polishing with 1-μm alumina, then colloidal silica.

Two measurements were made on the experimental run products, the

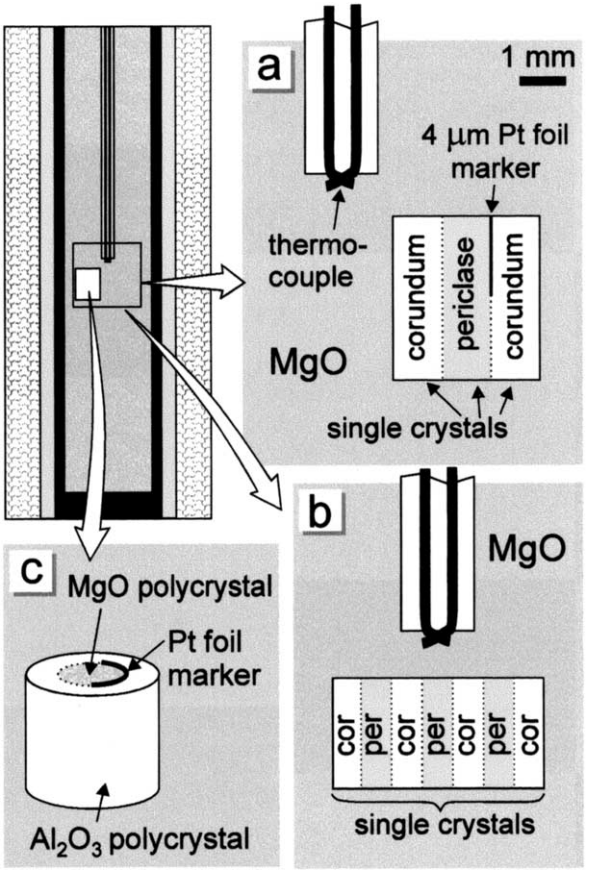

Fig. 2. Schematic representations of three specialized assembly configurations: (a) single-crystal "sandwich" of corundum and periclase surrounded by polycrystalline MgO, with Pt foil marker along part of one interface (run 48); (b) single-crystal, multilayer "sandwich" used in run 51 to deduce proportions of corundum and periclase consumed during spinel growth (see text and Figs. 3, 10, and 11); (c) coaxial cylinders of polycrystalline MgO and Al_2O_3, with Pt foil marker along portion of the interface (Fig. 10).

Table 1. Summary of run information, spinel layer thicknesses, and k values.

Experiment	T (°C)	P (GPa)	Duration (hr)	ΔX (μm)	k (m^2/sc)	$-\ln(k)$
54	1978	2.5	0.4	115	4.59E-12	26.11
53	1879	2.5	1.0	118	1.93E-12	26.97
52	1780	2.5	1.0	65	5.87E-13	28.16
18	1700	2.5	1.5	60	3.33E-13	28.73
19	1700	2.5	15.7	175	2.71E-13	28.94
20	1700	2.5	6.0	105	2.55E-13	29.00
29	1700	2.5	0.4	28	2.72E-13	28.93
36	1600	3.2	2.0	29	5.84E-14	30.47
39	1600	3.2	16.0	66	3.78E-14	30.91
9	1600	2.5	4.5	50	7.72E-14	30.19
12	1600	2.5	21.0	97	6.22E-14	30.41
13	1600	2.5	1.0	26	9.39E-14	30.00
14	1600	2.5	10.0	70	6.81E-14	30.32
15	1600	2.5	2.0	35	8.51E-14	30.10
25	1600	2.5	48.0	152	6.69E-14	30.34
34	1600	1.7	2.0	46	1.47E-13	29.55
40	1600	1.7	12.0	103	1.23E-13	29.73
37	1600	1.0	0.05	9	2.25E-13	29.12
42	1600	1.0	2.0	65	2.93E-13	28.86
17	1500	2.5	20.0	60	2.50E-14	31.32
21	1500	2.5	64.3	93	1.87E-14	31.61
22	1500	2.5	5.7	30	2.19E-14	31.45
26	1500	2.5	1.5	13	1.56E-14	31.79
51	1500	1.7	23.5	74	3.24E-14	31.06
50	1400	4.0	89.4	30	1.40E-15	34.20
35	1400	3.2	64.0	32	2.22E-15	33.74
38	1400	3.2	18.0	18	2.50E-15	33.62
10	1400	2.5	88.1	48	3.63E-15	33.25
27	1400	2.5	24.0	24	3.33E-15	33.34
30	1400	2.5	4.0	13	5.87E-15	32.77
32	1400	1.7	48.0	50	7.23E-15	32.56
33	1400	1.7	16.0	27	6.33E-15	32.69
47	1400	1.7	30.0	35	5.67E-15	32.80
48	1400	1.7	72.0	50	4.82E-15	32.97
23	1400	1.0	48.0	62	1.11E-14	32.13
41	1400	1.0	20.0	40	1.11E-14	32.13
11	1300	2.5	118.1	20	4.70E-16	35.29
28	1300	2.5	64.7	12	3.09E-16	35.71
31	1300	2.5	16.0	8	5.56E-16	35.13
49	1200	4.0	191.8	6	2.61E-17	38.19
44	1200	3.2	240.0	8	3.70E-17	37.84
16	1200	2.5	167.3	8	5.31E-17	37.47
46	1200	1.7	240.0	12.5	9.04E-17	36.94

first being simply the thickness of the spinel layer developed between contacting MgO and Al_2O_3. In most cases, these thickness determinations were made at the contact between the polycrystalline Al_2O_3 thermocouple insulator and the polycrystalline MgO filler pieces (Fig. 1). Because this contact surface is cylindrical, care was taken to be sure the true thickness of spinel was measured (i.e., that along a cylinder radius). Measurements were also made at planar MgO/Al_2O_3 contacts at various locations in the assemblies. As shown in Figure 2, these planar contacts were of several types: single-crystal Al_2O_3 against single-crystal MgO; single-crystal Al_2O_3 against dense MgO polycrystal; and dense Al_2O_3 polycrystal against dense MgO polycrystal. Three different methods were evaluated for suitability in gauging the thickness of the spinel layer. In order of increasing complexity, these were as follows: (1) visual estimates made with a micrometer ocular on a reflected-light optical microscope; (2) digital estimates from backscattered-electron (BSE) images obtained with the electron microprobe (EMP); and (3) digital estimates from X-ray raster maps, also obtained via EMP. The three techniques were found to give consistent results, so the simplest and least costly approach—the optical microscope—was adopted in those cases where thickness measurements alone were needed. Spinel thicknesses at curved and planar MgO/Al_2O_3 contacts in the same sample were found to be indistinguishable, thus eliminating concern about possible radial diffusion effects in the cylindrical geometry (the lack of a detectable three-dimensional geometric effect on diffusion, confirmed also by numerical calculations, is due to the large radius of curvature of the MgO/Al_2O_3 contact relative to the thickness of the spinel layer). Unless noted otherwise, all thicknesses reported here were obtained within 0.5 mm of the thermocouple—that is, within the "hot spot" of the piston-cylinder assembly. Spinel layer thickness decreased markedly moving away from the thermocouple, reflecting the thermal gradient within the assembly due to heat loss out the ends. The variation in spinel thickness with position in the assembly can be used to great advantage to map temperature distribution, as described by Watson et al. (2001).

The other analytical data acquired from the polished run products were EMP line traverses across the spinel layer formed during the experiments. Spinel deviates significantly from the ideal $MgAl_2O_4$ stoichiometry: in equilibrium with corundum, it contains an excess of Al^{3+} and a charge-compensating deficiency of Mg^{2+}, especially at temperatures above ~1600°C. In equilibrium with periclase, spinel contains a slight excess of Mg^{2+} accompanied by a deficiency in Al^{3+}. Knowledge of the gradients in Al and Mg from one interface to the other are crucial to the extraction of diffusivities, and the interface concentrations define the phase relations in the system. Accordingly, high-quality EMP results were obtained by crystal-dispersive methods with the JEOL 733 Superprobe at Rensselaer Polytechnic Institute; we used an accelerating voltage of 15 kV, a sample current of 30 to 35 nA,

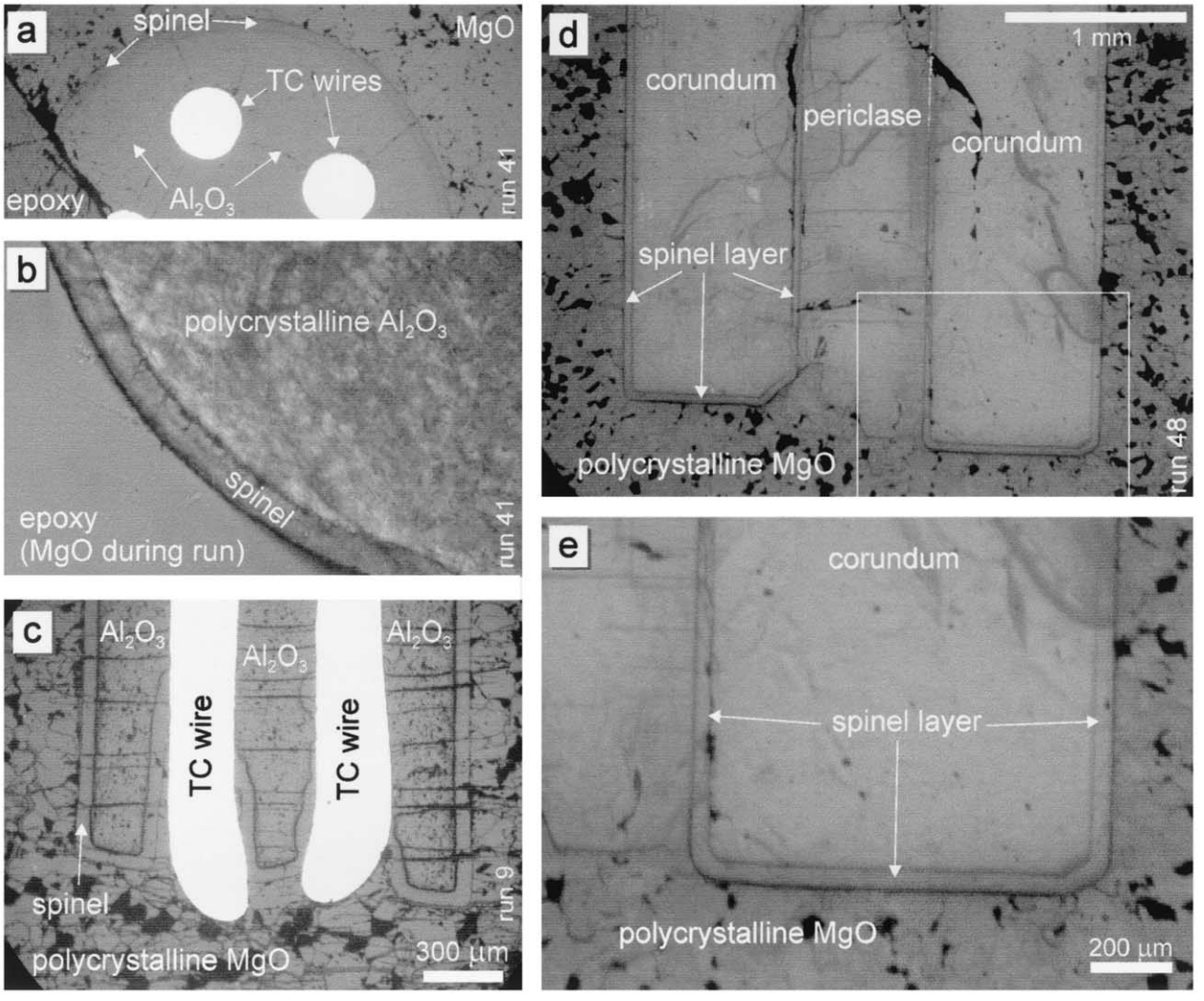

Fig. 3. Photomicrographs of run products showing various MgO/Al_2O_3 interfaces and resulting spinel layer. (a) Reflected-light image of Al_2O_3 thermocouple insulator sectioned just above the thermocouple tip of run 41 (wire diameter, ~250 μm); (b) transmitted-light image of spinel layer on Al_2O_3 in run 41; (c) reflected-light image of the region of the thermocouple tip in run 9; (d, e) reflected-light images of sectioned single-crystal "sandwich" in run 48.

a PET analyzing crystal, and a spot size of ~1.5 μm. The count rates on spinel were ~500 and ~200 cps for Al and Mg, respectively. Counting times of 80 to 120 s yielded detection limits of 0.05 wt% for Al_2O_3 and 0.07 wt% for MgO.

Because the EMP traverses included analyses close to the interface between two phases, it was necessary to demonstrate that secondary fluorescence did not contribute significantly to the X-ray intensities and apparent Mg and Al concentrations in the phases. A theoretical assessment of possible secondary fluorescence effects was made by examining tabulated X-ray generation and absorption characteristics in relevant model materials. This assessment predicted minimal secondary fluorescence contributions even at distances of 2 to 3 μm from an interface between phases. Two direct tests for secondary fluorescence were also conducted, first by preparing a blank couple consisting of periclase and corundum single crystals wired together, mounted in epoxy, and sectioned to expose an interface between the two at which no reaction or diffusion had occurred. Secondary fluorescence was not perceptible in analyses made very close to this interface: that is, no Mg X-rays were detected while sitting on Al_2O_3 at a distance of 2 to 3 μm from the interface, and vice versa. A second direct test involved traversing spinel layers from two experiments in which physical separation had fortuitously occurred at the interface between two phases—spinel from MgO in one experiment and spinel from Al_2O_3 in the other. The traverses yielded gradients indistinguishable from ones made across spinel layers still bonded to both of the other phases.

3. RESULTS

3.1. Spinel Development and Reaction Rate Constant

Selected photomicrographs of the periclase/corundum reaction zone are shown in Figure 3. Spinel layer thicknesses (ΔX) for all experiments are listed in Table 1 and plotted against the square root of run duration in Figure 4. In cases where the reacting phases were polycrystalline, the spinel layer shows minor irregularities but is of consistent thickness in a given region of the pressure assembly. At contacts involving reaction of single-crystal corundum with either single- or polycrystalline MgO, the spinel/corundum and spinel/periclase interfaces are extremely sharp and almost perfectly planar (Figs. 3d,e).

As in previous studies, spinel development shows a clear

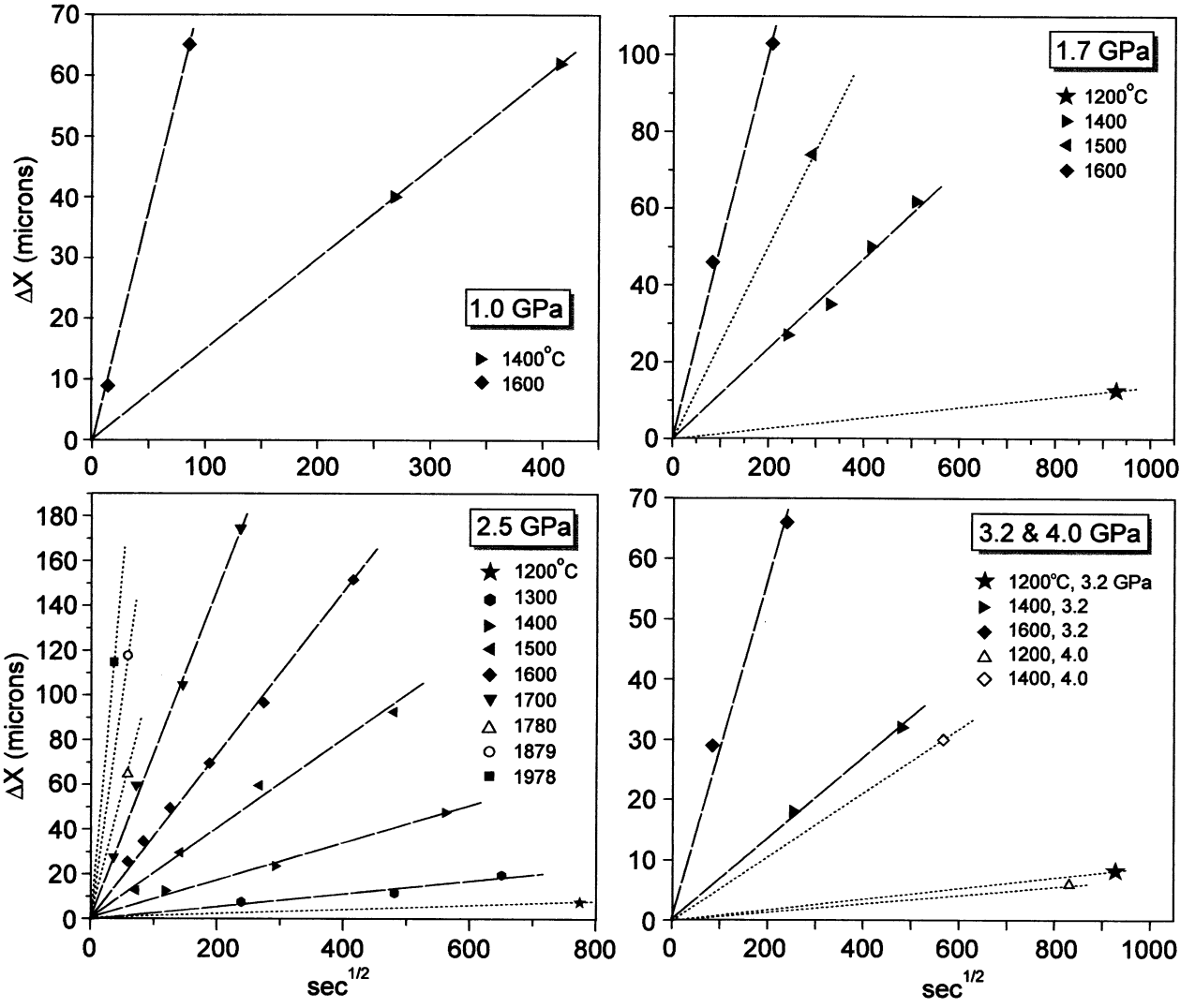

Fig. 4. Spinel layer thickness (ΔX) vs. the square root of run duration for experiments at 1.0, 1.7, 2.5, 3.2, and 4.0 GPa and a range of temperatures. The lines are constrained to pass through the origin; dotted lines are based on a single experiment.

parabolic dependence on time: data obtained from experiments at the same P-T conditions (i.e., differing only in duration) are arrayed along straight lines that generally pass through the origin in Figure 4. The effects of both temperature and pressure on spinel development are substantial and systematic.

In keeping with previous treatments following Tammann (1920), the spinel growth data were converted to a reaction rate constant, k, having the units of diffusivity

$$k = \frac{(\Delta X)^2}{2t}, \quad (1)$$

where ΔX is the thickness of the spinel layer and t is experiment duration. Calculated k values for each experiment are included in Table 1 and shown graphically as plots of ln(k)vs. $T(K)^{-1}$ and ln(k)vs. pressure (Figs. 5 and 6, respectively). Filled symbols are used in Figure 5 to highlight the 2.5-GPa data, which constitute the most comprehensive isobaric data set, extending over almost 800° (1200 to 1978°C) and including numerous variable-duration experiments at the same temperature. The coherence of the 2.5-GPa Arrhenius array is remarkable. Slight concave-downward curvature is suggested, but the slope of the regression line has an uncertainty of only ±1.7% at the 95% confidence level. Independent linear fits are included in Figure 5 for the other isobaric series at 1.0, 1.7, 2.5, 3.2, and 4.0 GPa. The effect of pressure is clear and systematic in the preexponential factors of the Arrhenius equations, but the slopes at different pressures are indistinguishable despite small uncertainties on three of them (see fit parameters on the figure). Because the rate constant k is not actually a diffusivity, the significance of the slopes—usually interpreted as activation energies—is uncertain. The rate constant includes a kinetic component related to diffusion through the spinel layer and a thermodynamic component related to the composition of spinel at the interfaces with Al_2O_3 and MgO (see section 3.2). The

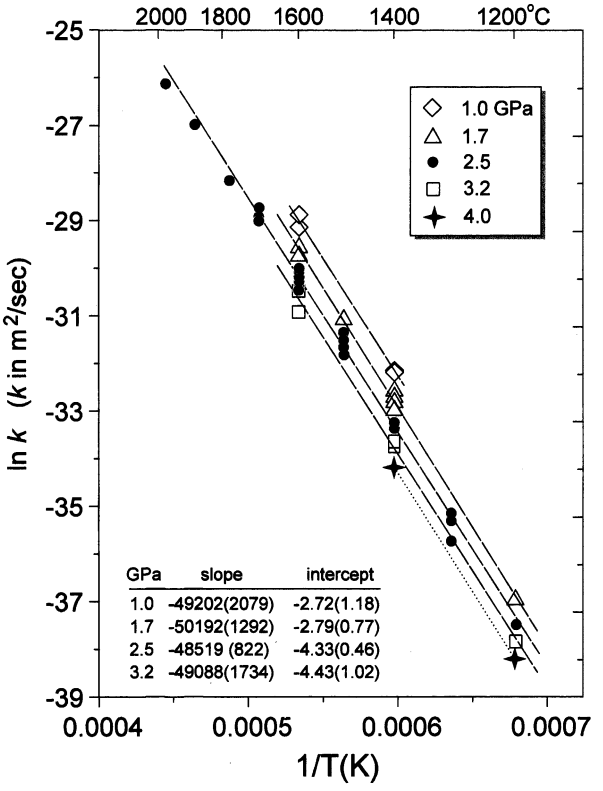

Fig. 5. Natural logarithm of the reaction rate constant ($k = \Delta X^2/2t$) vs. 1/T for all experiments. The dashed lines are linear regressions for isobaric series of data. Fit parameters are tabulated in the inset (2σ uncertainties indicated in parentheses).

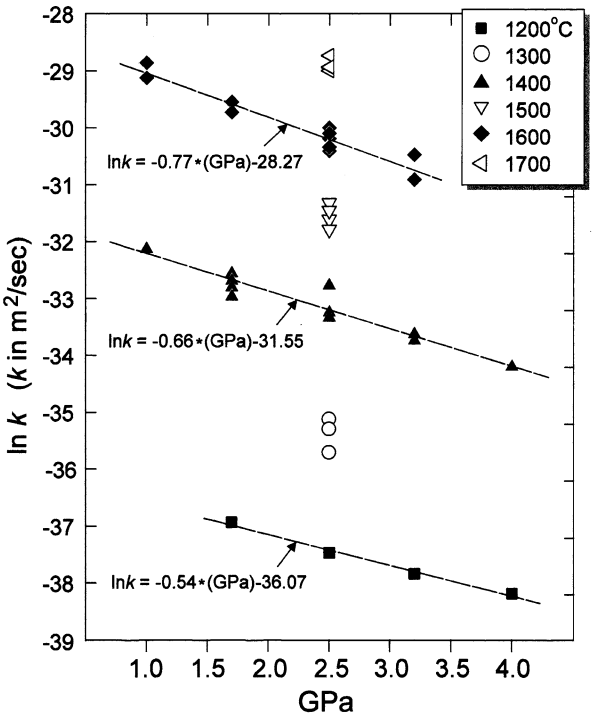

Fig. 6. Natural logarithm of the reaction rate constant ($k = \Delta X^2/2t$) vs. pressure in GPa for all experiments. The dashed lines are linear regressions for the three temperatures (1200, 1400, and 1600°C) at which polybaric data were obtained. The slopes are not expressed as activation volumes because the variation in k with pressure is later shown to be due to P-dependent phase relations in the MgO-Al_2O_3 system, not to an intrinsic effect of pressure on diffusion (see text).

apparent activation energy of the spinel growth process as described by k is nevertheless very well constrained at ~410 kJ/mol, which is independent of pressure within uncertainty. This value is somewhat lower than the ~540 kJ/mol of Zhang et al. (1996) for the temperature range 1200 to 1600°C. Whitney and Stubican (1971a) reported values of ~520 and 370 kJ/mol, respectively, for separate low- and high-temperature ranges of 1560 to 1750°C and 1750 to 1900°C. The temperature dependence of spinel growth is discussed more comprehensively in the section below devoted to Mg ↔ Al interdiffusion.

Variations in k with pressure (Fig. 6) are small in relation to temperature effects, but spinel growth clearly slows down systematically with increasing pressure. Inspection of Figure 4 reveals that a factor-of-two decrease in the thickness of the spinel layer can be brought about by a pressure increase of ~2 GPa or a temperature decrease of ~200°C.

3.2. Phase Compositions and Gradients

3.2.1. Microprobe Traverses, Interface Compositions, and the MgO-Al_2O_3 Phase Diagram

The main purpose of the EMP traverses was to characterize gradients in Mg and Al in the spinel layer formed between MgO and Al_2O_3 during high P-T treatment. However, because the compositions of all three phases might bear on the interpretation of the interdiffusion process, the traverses generally included short segments of corundum and periclase as well. Typical traverses are shown in Figure 7. From the standpoint of the phase equilibria, the information sought in the traverses was the compositions of the phases precisely at the interfaces. These compositions are not directly measurable, owing to the finite excitation volume of the EMP (~2 μm diameter) in combination with several other factors, including: small beam positioning uncertainties; sample relief developed during polishing (due to differing hardness of the phases); and occasional delamination cracks and plucking of grains. Reliable analyses were obtainable to within ~2 μm from the interfaces, and phase compositions precisely at the interfaces were estimated from short extrapolations of the analytical traverses. The method, illustrated in Figure 8, introduces a minor correction to interface compositions estimated simply on the basis of the "closest good analysis."

3.2.2. Spinel Composition

A consistent feature of all EMP traverses (see examples in Figs. 7 and 8) is the linear variation in the composition of the spinel layer across its width. At the interface with periclase, the spinel is nearly stoichiometric $MgAl_2O_4$, with only a slight Mg excess (Mg = 1.016 ± 0.016 atoms per four oxygens; Al = 1.99 ± 0.010) and no apparent dependence on temperature or pressure. At the interface with corundum, the spinel ranges from essentially stoichiometric $MgAl_2O_4$ at 1200°C to a significantly Mg-deficient composition at higher temperatures, with Mg values

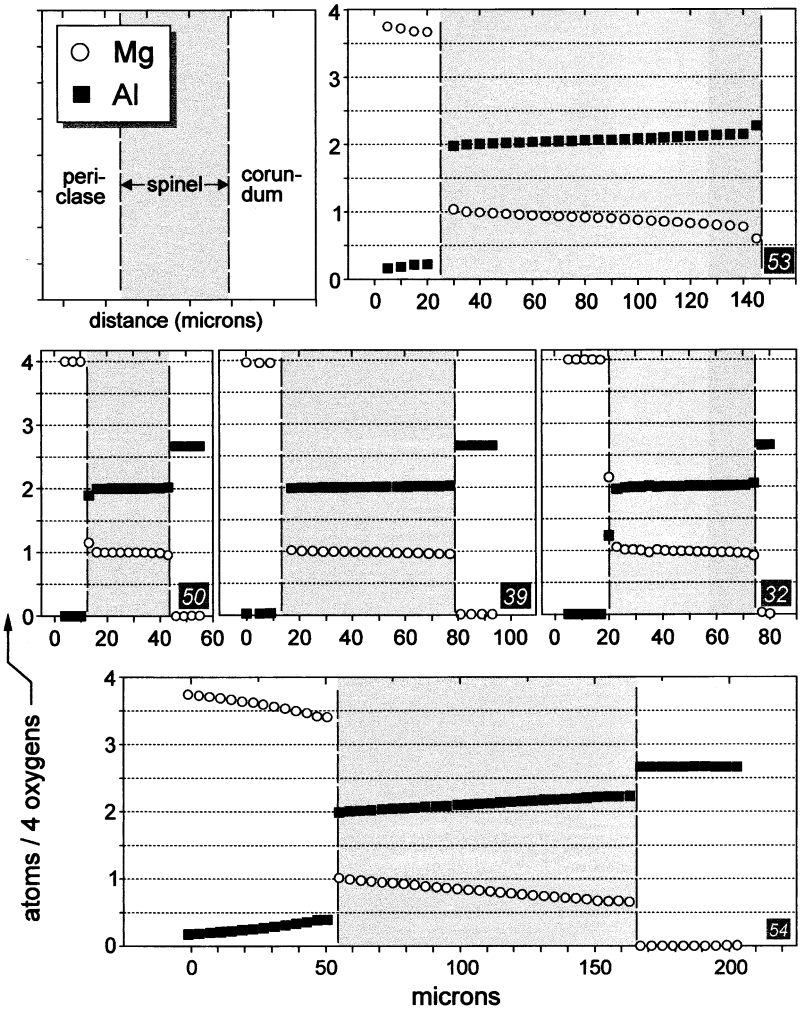

Fig. 7. Selected EMP traverses across the spinel layer in several run products (runs 32, 39, 50, 53, and 54; see lower right corner of each panel). The uncertainties in each analysis fall within the symbols (see analytical details in the text). The distance scales are the same for the five plots.

as low as 0.634 (Al = 2.244) at 1978°C and 2.5 GPa (see data summarized in Table 2). As required by charge balance in the spinel structure, an Mg^{2+} deficit of a given magnitude is compensated by an Al^{3+} excess of exactly two-thirds that magnitude. This point is convincingly demonstrated by the fact that the ratios of the slopes of the linear Al and Mg profiles is -0.668 ± 0.006 for the 18 traverses that have measurable slopes (the three runs at 1200°C and the 4-GPa run at 1400°C have slopes very close to zero, with consequent large uncertainties; Table 2). The constraints of stoichiometry and charge balance require that spinel in equilibrium with corundum have vacant cation sites accordingly to the formula $Mg_{1-3x}\ Al_{2+2x}\square_xO_4$, where $\square$ is a cation vacancy. The cation total (Al + Mg atoms per four oxygens) for spinel coexisting with MgO is 3.006 ± 0.004; in contrast, Al + Mg in spinels coexisting with corundum ranges down to 2.878 at 1978°C and 2.5 GPa. In this extreme case, $x = 0.122$, meaning that 4% of all cation sites are unoccupied. The distribution of cation vacancies between the tetrahedral and octahedral sites cannot be determined from our data.

The composition of spinel coexisting with corundum varies systematically as a function of both temperature and pressure (Fig. 9), with the maximum deviations from stoichiometry (excess Al) occurring at high temperatures and low pressures. As shown in Figure 9a, the pressure effect is pronounced at 1400 to 1600°C and leads to the near elimination of excess Al at the 4-GPa maximum pressure of this study. As demonstrated in previous studies conducted at atmospheric pressure (e.g., Alper et al., 1962; Zhang et al., 1996), temperatures in excess of ~1400°C can result in significant solubility of "excess" Al_2O_3 in spinel (Fig. 9b), but this effect is reduced dramatically at high pressures (see p. 2109 of Zhang et al., 1996, for a discussion of previous information on the composition of spinel in equilibrium with periclase and corundum at 1 atm pressure).

3.2.3. Periclase and Corundum Compositions

As noted above, the compositions of periclase and corundum were not a primary focus of this study, but some insight into the solubility of Al_2O_3 in periclase and MgO in corundum at high P-T conditions can be gained from the EMP traverses. The

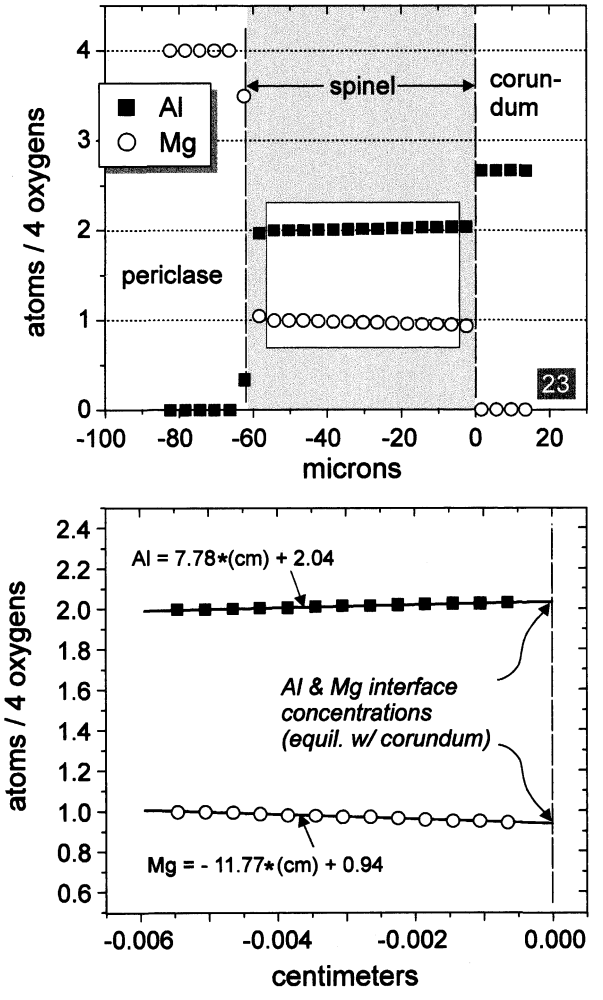

Fig. 8. Illustration of the method used to determine the composition of spinel at the interfaces with corundum and periclase, and to define the slopes of the linear concentration profiles of Al and Mg across the spinel layer (run 23 is used as an example). For reasons given in the text, EMP analyses made within a few microns of the interfaces are not considered reliable, so only the "good" data—outlined by the white rectangle in the top panel—are used to compute slopes and intercepts as shown in the bottom panel. Note that the ratio of the Al and Mg slopes is −0.661; the intercepts (2.04 and 0.94 for Al and Mg, respectively) represent the composition of spinel in equilibrium with corundum because the corundum/spinel interface is set as $x = 0$.

most complete set of data on periclase composition is for the 2.5-GPa series. At temperatures below ~1600°C, periclase in equilibrium with spinel is nearly pure MgO, but appreciable amounts of Al are incorporated at temperatures in excess of 1700°C, rising to Al/(Al + Mg) ~ 0.1 at 1978°C (Fig. 9c). Comparison of the 2.5-GPa data with lower pressure data suggests that any effect of pressure is small: at 1.0 GPa and 1600°C, Al/(Al + Mg) in periclase is ~0.017, which is comparable with the 2.5-GPa value of ~0.014. The composition of corundum is nominally pure over the entire range of P-T conditions investigated, with Mg never exceeding 0.01 atoms per four oxygens even at the highest temperatures investigated. Our overall compositional systematics are in qualitative agreement with those summarized in Zhang et al. (1996; see their fig. 4). Their summary includes no data above ~1600°C and no high-pressure information, but allowance for these differences suggests general consistency of the compositional trends.

3.3. Volume Changes, Interface Positions, and Fluxes

A remaining obstacle to understanding the nature of the diffusion processes governing spinel growth concerns the manner and direction in which the spinel layer grows relative to the original MgO/Al_2O_3 boundary. This general problem can be broken down into a series of simpler questions related to mass transfer in the interfacial region.

The first question concerns the amount of corundum and periclase consumed during spinel growth, which can be estimated from molar volume considerations assuming all phases are stoichiometric and pure (i.e., corundum = Al_2O_3; periclase = MgO; spinel = $MgAl_2O_4$). Spinel grows in one dimension only, so measurements of the widths of the phases in sections perpendicular to the interface should accurately reflect volumetric changes (this is strictly true only for cubic phases and polycrystals with random grain orientation). The 1-atm molar volumes of corundum (Al_2O_3), periclase (MgO) and spinel ($MgAl_2O_4$) are 25.58, 11.25 and 39.71 cm^3, respectively (Robie et al., 1978), so ΔV for the reaction *periclase + corundum → spinel* is +2.88 cm^3/mol. The linear amount of corundum consumed is predicted to be 64.4% of the width of the spinel layer; similarly, the amount of periclase consumed should be 28.3% of the width of the spinel layer (assuming the relevant molar volumes are insensitive to changes in pressure). As a check for consistency between these predictions and the actual behavior of the system, a technique was devised to allow direct characterization of corundum consumption during the experiments. In two experiments, polished slabs of single-crystal corundum were stacked with crystals of periclase in multi-layer "sandwiches." Run 48 (1400°C, 1.7 GPa) included two corundum slabs, each ~930 μm thick, separated by a single crystal of periclase and surrounded by polycrystalline periclase (Figs. 2a and 3d,e). Run 51 (1500°C, 1.7GPa) consisted of four corundum slabs, each ~500 μm thick, also separated by periclase single crystals (Figs. 2b and 10). In both cases the thicknesses of the corundum slabs were measured before the experiments so the amount consumed could be calculated from postexperiment measurements. No attempts were made to quantify periclase consumption because mechanical deformation of this softer phase obscured the expected small thickness changes. The thickness lost from each side of the corundum slabs in run 48 is 64.0% of the adjacent spinel layer thickness. This is almost exactly (and probably fortuitously) the same as the 64.4% estimated from the 1-atm ΔV data. For run 51 the data are not quite as satisfying, with consumed corundum averaging 73.5% of the spinel layer thickness. The explanation for the discrepancy probably lies in the higher temperature of this run. As temperature increases, spinel coexisting with corundum takes in progressively larger amounts of excess Al_2O_3 (i.e., above stoichiometric $MgAl_2O_4$; Fig. 9a). Calculations based on molar volumes that assume stoichiometric spinel would thus underestimate the amount of corundum consumed, an effect magnified by the greater thickness of the spinel layer in run 51 (relative to run 48). On the whole, the results indicate that the observed amount of spinel

Table 2. Summary of information pertaining to the diffusivities calculated using the approach illustrated in Figures 8 and 13 in combination with Eq. 15.[a]

Experiment	T (°C)	P (GPa)	$C^{sp}_{All}\mid_{cor}$	$C^{sp}_{Mg}\mid_{cor}$	$\Delta C^{sp}_{All}/\Delta x$	$-\log(\tilde{D})$
54a	1978	2.5	0.05641 (4.2E-5)	0.01610 (6.7E-5)	−0.57736 (.007)	11.06
54b	1978	2.5	0.05650 (4.2E-5)	0.01597 (5.9E-5)	−0.56275 (.006)	11.05
53	1879	2.5	0.05417 (5.0E-5)	0.01947 (7.6E-5)	−0.34803 (.008)	11.23
52	1780	2.5	0.05303 (6.7E-5)	0.02129 (6.7E-5)	−0.49150 (.018)	11.64
18	1700	2.5	0.05245 (3.4E-5)	0.02205 (3.4E-5)	−0.39688 (.009)	11.75
39	1600	3.2	0.05105 (1.7E-5)	0.02412 (2.5E-5)	−0.14690 (.005)	12.31
15	1600	2.5	0.05149 (3.4E-5)	0.02349 (5.0E-5)	−0.37397 (.016)	12.09
34	1600	1.7	0.05247 (1.7E-5)	0.02198 (2.5E-5)	−0.46773 (.005)	12.57
42	1600	1.0	0.05382 (4.2E-5)	0.02000 (6.7E-5)	−0.55965 (.011)	11.99
17	1500	2.5	0.05112 (2.5E-5)	0.02402 (3.4E-5)	−0.16411 (.008)	12.49
22	1500	2.5	0.05118 (5.9E-5)	0.02401 (1.0E-4)	−0.46169 (.042)	12.70
26	1500	2.5	0.05107 (4.2E-5)	0.02419 (9.2E-5)	−0.72753 (.056)	12.68
50	1400	4.0	0.05047 (2.5E-5)	0.02506 (3.4E-5)	−0.06531 (.012)	13.05
35	1400	3.2	0.05050 (3.4E-5)	0.02502 (4.2E-5)	−0.10661 (.021)	13.09
10	1400	2.5	0.05063 (2.5E-5)	0.02479 (4.2E-5)	−0.13060 (.010)	13.14
32	1400	1.7	0.05100 (5.9E-5)	0.02420 (1.0E-4)	−0.16167 (.021)	12.95
23	1400	1.0	0.05142 (2.5E-5)	0.02360 (4.2E-5)	−0.20524 (.008)	12.96
11	1300	2.5	0.05032 (4.2E-5)	0.02522 (4.2E-5)	−0.04990 (.047)	13.23

[a] Symbols are the same as those used in the text. The units of concentration (C) are mole/cm^3; subscripts identify the element, superscripts the phase ("cor" refers to spinel composition at the interface with corundum). Distance is in cm; diffusivity is in m^2/s. The value in parentheses are the 2σ uncertainties on the slope and intercepts indicated in Figure 8 (see test).

growth is generally consistent with tabulated volumetric data for the relevant minerals.

Reactant consumption tells us little about the directions and magnitudes of component fluxes in the interfacial region. Here, a key question concerns the location of the original MgO/Al_2O_3 interface relative to the newly grown spinel layer. The Pt foil inserted to mark the original boundary in several experiments (see section 2) yielded a generally consistent result in this regard: in almost every instance, the Pt marker remained in contact with periclase (Fig. 11). Because periclase is consumed in making spinel, this adherence of the Pt marker to the periclase/spinel boundary indicates that the Pt marker moves relative to the (assumed) fixed position of the original periclase/corundum contact. This could be interpreted to mean that spinel growth occurs only at the spinel/corundum interface, "fed" by diffusion of both Mg and O through the spinel layer (but see below). A particularly interesting aspect of the Pt foil marker experiments is that spinel development appears unhindered by the presence of the foil, suggesting that Mg and O atoms actually diffuse through it. This possibility is given credence by the fact that the foil recrystallizes at run conditions into necklace-like structures or "bleb chains" that appear only semicontinuous and therefore "permeable" to diffusion (Fig. 11).

The last piece of evidence concerning component fluxes and interface positions comes from high-contrast BSE images of the spinel layer itself. Four such images are shown in Figure 12 (run 48), which reveal that the spinel layer grown between single-crystal corundum and periclase (both single-crystal and polycrystal) actually comprises two microstructurally distinct sublayers. The spinel grains in the layer contacting periclase are generally no larger than 5 μm in any dimension and are relatively equidimensional. In contrast, the spinel grains contacting corundum are much larger and exhibit preferred elongation perpendicular to the interface, forming a "comb" structure that appears to extend across the entire sublayer (see especially Fig. 12b). The demarcation between the two sublayers of spinel is planar and sharp. For a total spinel layer thickness ΔX, the sublayers are consistently $\frac{1}{4}\Delta X$ and $\frac{3}{4}\Delta X$ in thickness, respectively, for the fine-grained layer against periclase and the comb-structured layer against corundum. It is difficult to envision any explanation for the existence of the sublayers other than that they reflect spinel grown by consumption of periclase on one side ($\frac{1}{4}\Delta X$) and corundum on the other ($\frac{3}{4}\Delta X$). Growth only at the spinel/corundum contact—supplied by diffusion of Mg and O through the spinel—seems inconsistent with the existence of distinct spinel sublayers. If this interpretation is correct, then the boundary between the sublayers is positionally equivalent, in a fixed reference frame, to the original periclase/corundum interface. This conclusion is greatly strengthened by one anomalous instance in which the edge of the Pt foil remained pinned at the interface between the spinel sublayers (Fig. 12b; cf. Fig. 12a), apparently serving its intended purpose as an immobile marker. The photo reveals bifurcation and smearing of the Pt, but there is clearly spinel on both sides of it.

3.4. Diffusion Model and Mg=Al Interdiffusion Coefficients

The Mg and Al analyses of the spinel layers, in combination with the observations in the preceding section, suggest a simple diffusion model. The linear character of the EMP analytical profiles and the well-constrained $-2/3$ ratio of their slopes (Al/Mg) indicate first that the diffusivity governing the interdiffusion process is not a function of distance across the spinel (i.e., of spinel composition), and second that charge balance in the spinel is maintained by counterfluxes of Mg and Al atoms in a ratio of two Al^{3+} ions for every three Mg^{2+} ions. From these observations, it follows that spinel grows in both directions: at the spinel/corundum interface via a flux of Mg^{2+} ions from periclase and at the spinel/periclase interface via a flux of Al^{3+} ions from corundum. Because these counterfluxes have a simple and fixed relationship to one another ($-3/2$), the growth

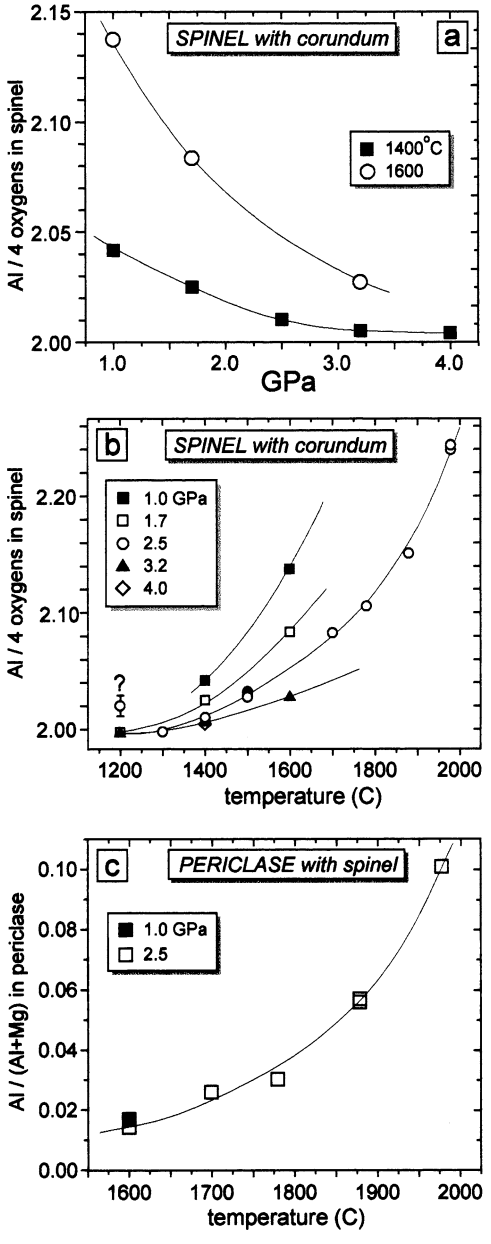

Fig. 9. Representation of phase relations in the MgO-Al_2O_3 system in terms of compositional variations of coexisting phases as a function of temperature and pressure. (a) Spinel coexisting with corundum as a function of pressure at 1400 and 1600°C; (b) spinel coexisting with corundum as a function of temperature at 1.0, 1.7, 2.5, 3.2, and 4.0 GPa; (c) composition of periclase coexisting with spinel as a function of temperature at 2.5 GPa (1 datum at 1.0 GPa).

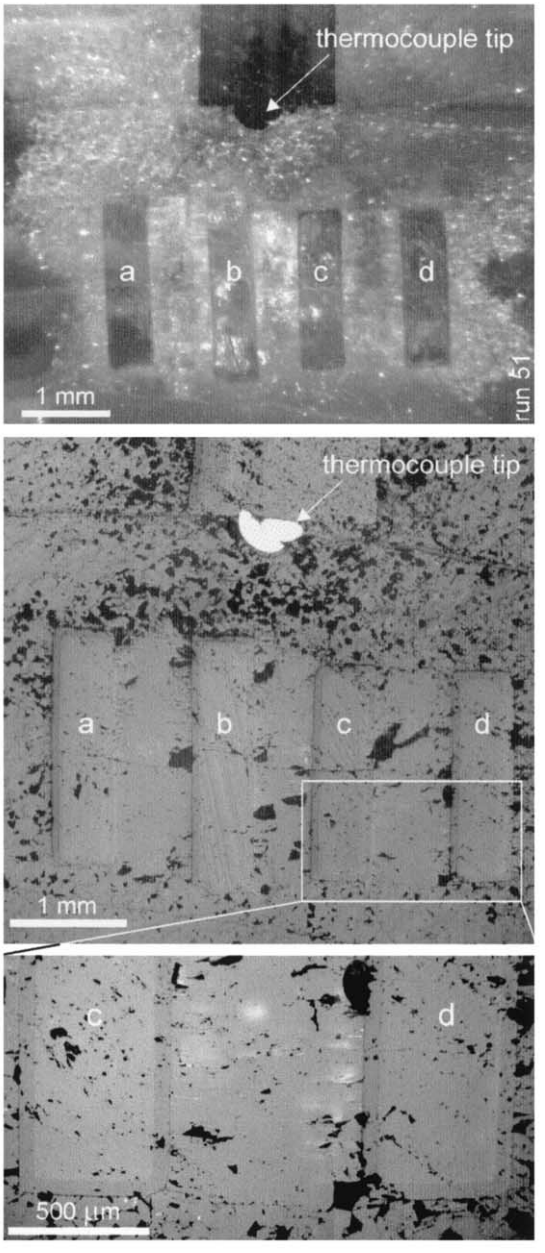

Fig. 10. Reflected-light photomicrographs of the sectioned and polished multilayer "sandwich" of periclase and corundum single crystals in run 51 (illumination is oblique in the top panel and vertical in the middle and bottom panels). The rectangles labeled a to d are the four corundum slabs (with spinel reaction rims) from which the proportion of corundum consumed (relative to periclase) during spinel growth was deduced quantitatively. See text.

rates of spinel at the two interfaces must also be related in a simple way. Growth of spinel by consumption of periclase at the spinel/periclase interface is determined by the supply rate of Al atoms via diffusion through the spinel (J_{Al}^{sp}) and occurs at rate given by

$$V_{per} = \frac{J_{Al}^{sp}}{C_{Al}^{sp} - C_{Al}^{per}}, \quad (2)$$

where V_{per} is the linear rate of spinel growth into periclase, and C_{Al}^{sp} and C_{Al}^{per} are the concentrations of Al in spinel and periclase, respectively (mol/cm^3). Recognizing that C_{Al}^{per} is very small except at the highest temperatures investigated (see section 3.2.3), this expression simplifies to

$$V_{per} = \frac{J_{Al}^{sp}}{C_{Al}^{sp}}. \quad (3)$$

By similar reasoning, the linear growth rate of spinel into

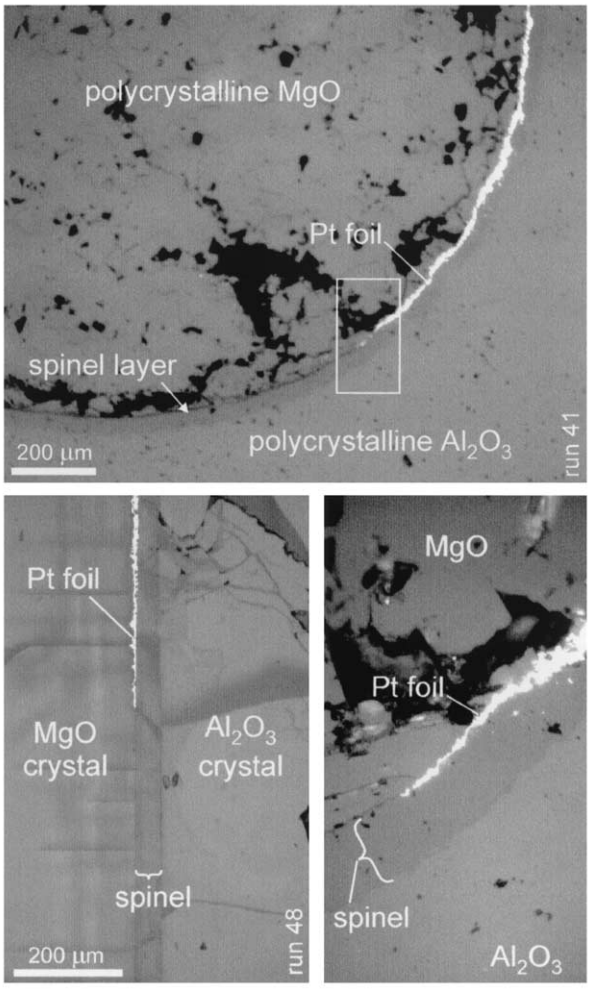

Fig. 11. Reflected-light photomicrographs of the Pt foil marker in two run products. (top) Spinel layer between polycrystalline MgO and Al_2O_3 in run 41; the critical region that includes the edge of the Pt marker is enlarged in the lower right panel. (bottom left) Single crystals of MgO and Al_2O_3 (with decompression cracks) in run 48, separated by spinel. The Pt foil marker projects down from the top. Note that the Pt marker (placed at the prereaction periclase/corundum interface) "adheres" to the periclase/spinel interface in both experiments. The suggestion—subsequently proved incorrect—is that the spinel grows by consumption only of corundum (see text and Figs. 11 to 13). See also Figure 12b for the one documented instance in which the Pt marker does not adhere to the periclase/spinel interface.

corundum (V_{cor}), determined by the supply of Mg atoms to the spinel/corundum interface, is given by

$$V_{cor} = \frac{J^{sp}_{Mg}}{C^{sp}_{Mg}}. \quad (4)$$

Charge balance requires, and the analytical data show, that $J^{sp}_{Mg} = -1.5 \times J^{sp}_{Al}$. The additional constraint that $C^{sp}_{Mg} \cong 0.5 \times C^{sp}_{Al}$ in $MgAl_2O_4$ leads to the result that

$$V_{cor} = \frac{-1.5J^{sp}_{Al}}{0.5C^{sp}_{Al}} = -3V_{per}. \quad (5)$$

Corundum is consumed by spinel growth at a rate three times as fast as periclase (i.e., 75% of total spinel growth is by consumption of corundum). This conclusion is exactly borne out by the spinel sublayer evidence (Fig. 12; see section 3.3). The reaction occurring at the spinel/corundum interface is

$$3Mg^{2+} + 4Al_2O_3 \rightarrow 2A1^{3+} + 3MgAl_2O_4,$$

and that at the spinel/periclase interface is

$$2Al^{3+} + 4MgO \rightarrow 3Mg^{2+} + MgAl_2O_4.$$

These reactions are balanced with respect to one another in terms of the ion fluxes through the spinel; note again that the amount of spinel produced at the spinel/corundum interface is three times that produced at the spinel/periclase interface.

The model of spinel growth described above is illustrated in Figure 13. The instantaneous fluxes, reactions, and relevant distance parameters are shown in Figure 13a, and the expected time evolution is depicted schematically in Figure 13b. The manner in which the compositional profiles change with time is crucial to the arguments made here because it shows that both Mg and Al are mobile. Taken in isolation, the vast majority of the Pt marker results could be interpreted to mean that Mg and O diffuse across the spinel layer to supply its growth at the spinel/corundum interface. As noted previously, the layered microstructure of the spinel provides a strong counter-argument to this view, but confirming chemical evidence of Al mobility is also helpful. Figure 13b shows that the combined constraints of partitioning equilibrium at the two interfaces and linear concentration gradients across a growing spinel layer require that local Al concentrations must change with time. The spinel sublayer evidence argues against this change being due simply to "dilution" by Mg and O.

The model illustrated in Figure 13 also serves as a basis for a simple scheme to calculate Mg ↔ Al interdiffusion coefficients in the spinel layer. The linear concentration profiles of Al and Mg require that the instantaneous fluxes of these components at all locations in the spinel layer are given by

$$J_{Al} = -\tilde{D}\frac{\Delta C^{sp}_{Al}}{\Delta x} \quad (6)$$

and

$$J_{Mg} = -\tilde{D}\frac{\Delta C^{sp}_{Mg}}{\Delta x}, \quad (7)$$

where $\tilde{D}$ is the Mg-Al interdiffusion coefficient and x is distance perpendicular to the interfaces. As noted above, J_{Mg} and J_{Al} are opposite but not equal because of the "three-for-two" charge-balance constraint on the interdiffusion process. The diffusivity can be calculated from the concentration profile of either Mg or Al. The Al profile is used here because the EMP analyses for Al in spinel are slightly better; it seems likely also that Al^{3+} is the rate-controlling species in the interdiffusion process. Recall that the flux of Al through the spinel leads to consumption of periclase at the spinel/periclase interface. During a diffusion anneal, the rate of spinel growth by periclase consumption is

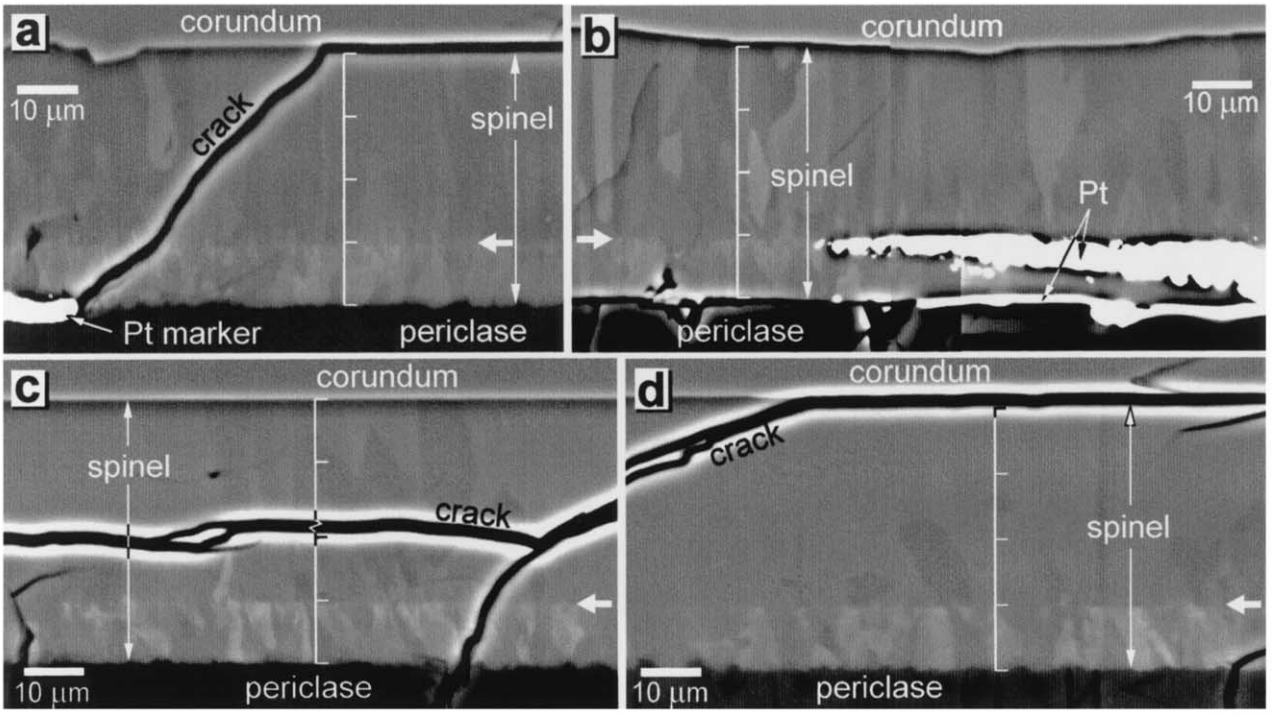

Fig. 12. High-contrast BSE images of the spinel layer produced in run 48 by reaction of single-crystal corundum (at the top in all photos) with either polycrystalline (a, b) or single-crystal periclase (c, d). All photos reveal two microstructurally distinct sublayers of polycrystalline spinel separated by a planar interface (white arrows). Note that spinel grown from periclase (at bottom) is fine grained and randomly oriented in comparison with the coarse, "comb"-textured spinel grown from corundum (the latter is most apparent in b). Panels (a) and (b) both include the edge of the Pt foil marker (white) but show different behaviors: in (a), the Pt marker resides at the spinel/corundum interface (as is typical; Fig. 11); in (b), however, the edge of the Pt foil remains at the interface between the two spinel sublayers. According to our interdiffusion model for spinel growth, the sublayer boundary marks the original periclase/corundum interface (see text and Fig. 13). The white line with tick marks at a quarter, half, and three-quarters of its length shows that the sublayer widths are close to a 25:75 ratio.

$$\frac{dW_{per}}{dt} = \frac{J^{sp}_{Al}}{C^{sp}_{Al}|_{per}} \quad (= V_{per}), \tag{8}$$

where $C^{sp}_{Al}|_{per}$ is the concentration of Al in spinel (mol/cm^3) at the spinel/periclase interface. The width of spinel grown in a given time by periclase consumption (W_{per}) is related to the total spinel grown (ΔX) as shown above: $W_{per} = \Delta X/4$, where ΔX is one of the quantities actually measured in the experiments (see section 3.1). In keeping with the rate-constant formulation used previously, W_{per} is a known function of time:

$$W_{per} = \frac{(2kt)^{1/2}}{4} \tag{9}$$

$$\frac{dW_{per}}{dt} = \frac{\sqrt{2} \times k}{8(kt)^{1/2}}. \tag{10}$$

Substituting from Eqn. 8,

$$\frac{J^{sp}_{Al}}{C^{sp}_{Al}|_{per}} = \frac{\sqrt{2} \times k}{8(kt)^{1/2}}, \tag{11}$$

and recognizing that the instantaneous Al flux in spinal is given by

$$J^{sp}_{Al} = -\tilde{D}\,\frac{\Delta C^{sp}_{Al}}{\Delta x}, \tag{12}$$

we arrive at

$$\frac{\tilde{D}\,\dfrac{\Delta C^{sp}_{Al}}{\Delta x}}{C^{sp}_{Al}|_{per}} = -\frac{\sqrt{2} \times k}{8(kt)^{1/2}}, \tag{13}$$

which can be rearranged into the usable form

$$\tilde{D} = -C^{sp}_{Al}|_{per} \times \frac{\sqrt{2} \times k}{8(kt)^{1/2}} \times \frac{\Delta x}{\Delta C^{sp}_{Al}}. \tag{14}$$

Eqn. 14 enables calculation of $\tilde{D}$ from a single EMP traverse to obtain the slope of the concentration profile ($\Delta x/\Delta C^{sp}_{Al}$, where x is distance). Use of the equation is made easier by the fact that the composition of spinel in equilibrium with periclase (hence $C^{sp}_{Al}|_{per}$) is essentially invariant at $MgAl_2O_4$ (see section 3.2.2). At STP, the molar volume of spinel is 39.71 cm^3 (Robie et al., 1978), which leads to an Al concentration of 0.0504 mol/cm^3. This value could be adjusted for compression and thermal expansion of spinel at the conditions of the experiments, but considering the other approximations made in the analysis and

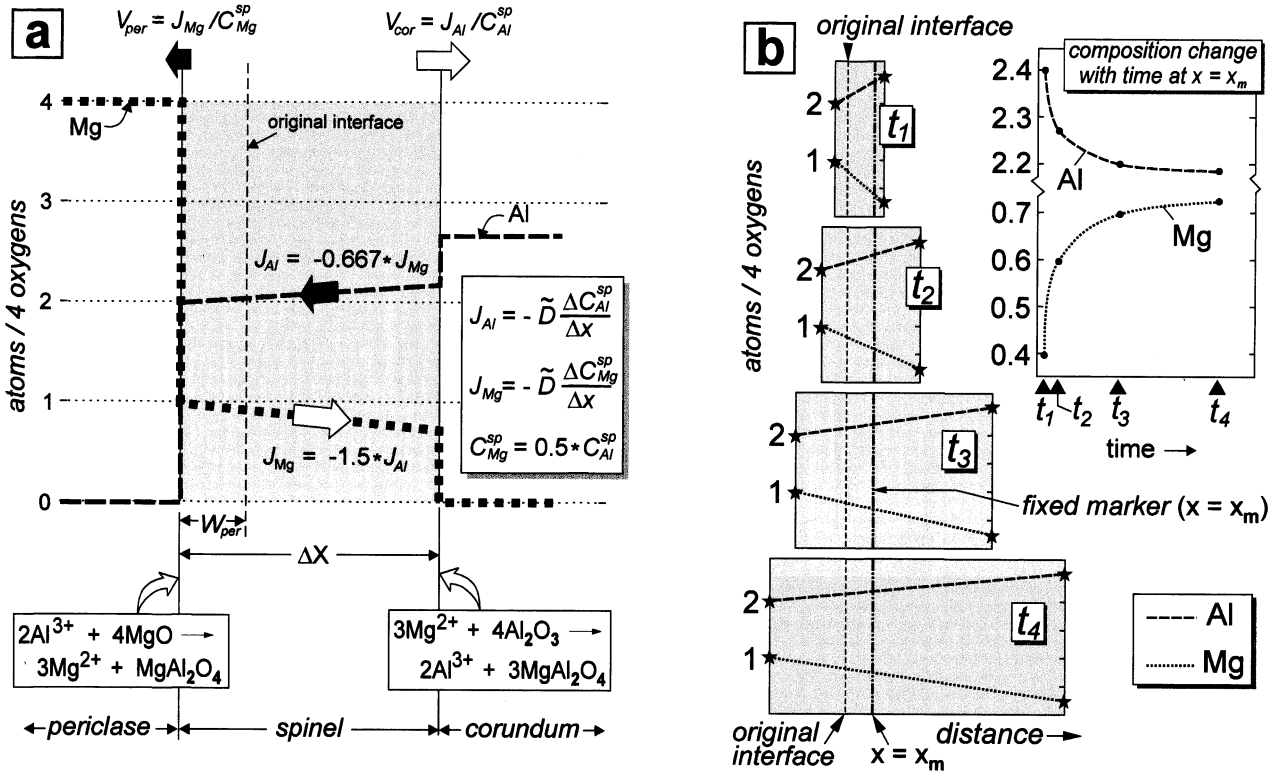

Fig. 13. Schematic representations of spinel growth between periclase and corundum via Mg ↔ Al exchange through spinel, as deduced from the EMP analyses and the two-layer structure of the spinel (see text and Fig. 12). (a) Instantaneous fluxes and interface reactions. (b) Spinel growth with time in a series of four steps (t_1 to t_4); star symbols mark the time-independent interface concentrations determined by partitioning equilibrium (Fig. 9). The graph at the upper right in (b) shows the time evolution (as $t_1 \rightarrow t_4$) of Al and Mg concentrations in spinel at an arbitrary fixed marker within the spinel layer (vertical dash-dot line at $x = x_m$). For clarity, the hypothetical concentration gradients depicted are near the high end of the range seen in the actual experiments (Fig. 7). See text for discussion.

the uncertain value of any gains in accuracy, such fine-tuning is considered unwarranted for the purposes of this article. The fact that k is known to be independent of time (Figs. 4 to 6) imparts greater confidence in the approach than would be warranted in basing a diffusivity value on a single experiment. If the time independence of k is accepted a priori, however, replacing k in Eqn. 14 by $\Delta X^2/2t$ (Eqn. 1) gives the simple result

$$\tilde{D} = -\frac{C^{sp}_{Al|_{per}}}{\Delta C^{sp}_{Al}*} \times \frac{\Delta X^2}{8t}, \qquad (15)$$

where $\Delta C^{sp^*}_{Al}$ is the difference in Al concentration in spinel (in mol/cm^3) across the full width of the spinel layer.

It is clear from the above analysis and the EMP traverses on which it is based that the temperature dependence of spinel growth as represented by k is actually a convolution of two effects: the intrinsic effect of temperature on $\tilde{D}$ and the sensitivity of the spinel-corundum phase relations to temperature. The increasing solubility of Al in spinel with increasing temperature (especially above ~1500°C) steepens the concentration gradients driving diffusion, so the fluxes would increase (and spinel would grow faster) even for a fixed value of $\tilde{D}$. Put another way, the difference in chemical potentials of Al in spinel coexisting with corundum on the one hand and with periclase on the other diverge significantly with increasing temperature. The positive temperature dependence of "$\Delta\mu^{per/cor}_{Al}$" augments the intrinsic effect of temperature on $\tilde{D}$ to markedly increase the growth rate of spinel at high temperatures.

The interdiffusion coefficients calculated by the method outlined above are summarized on an Arrhenius-type plot in Figure 14. The time independence of computed $\tilde{D}$ values is confirmed in Figure 15, which reveals similar diffusivities for three experiments at 1500°C differing in duration by a factor of ~15. The error estimates shown on the figures were obtained solely from the uncertainty (at 95% confidence) in the $\Delta x/\Delta C^{sp}_{Al}$ term in the equation (Eqns. 14 or 15) used to compute $\tilde{D}$ (Figs. 8 and 13, Table 2). This slope is the main contributor to the overall uncertainty in the diffusivity, which is small at high temperatures but increasingly serious at 1300 and 1200°C. The large uncertainty in $\tilde{D}$ at 1300°C is shown on the figure; the uncertainties at 1200° are so large that the diffusivities are of little value, so they are not plotted. A linear fit to log$\tilde{D}$ vs. T^{-1} at 2.5 GPa over the temperature range 1300 to 1978°C (solid line in Fig. 14) reveals an activation energy for Al ↔ Mg interdiffusion of 234 kJ/mol.

Two additional Arrhenius lines describing the temperature dependence of log($\tilde{D}$) are included in Figure 14. One of these (the dotted line) was obtained by Zhang et al. (1996) using the analytical solution of Wagner (1969) to calculate $\tilde{D}$ from EMP

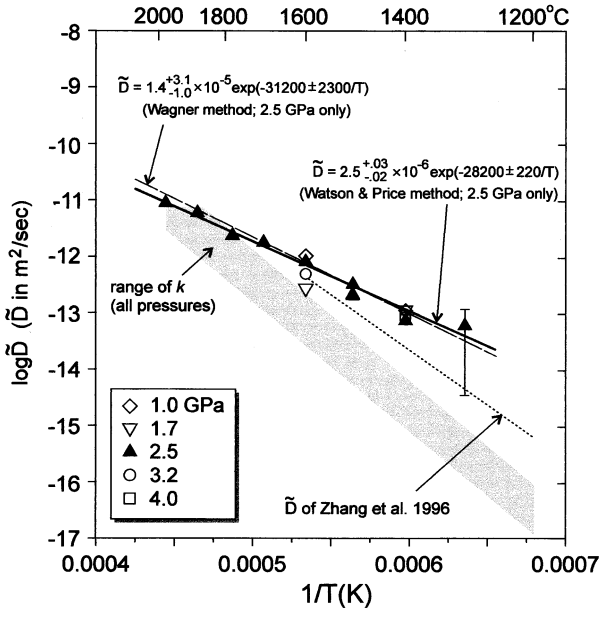

Fig. 14. Logarithm of the diffusivity ($\tilde{D}$) for Mg ↔ Al exchange in spinel vs. 1/T. The diffusivities were calculated from the present experiments by the simplified model represented by Eqn. 14 (solid line) and also by using Wagner's (1969) rigorous solution to the non–steady-state diffusion equation (dashed line). See text for further discussion.

traverses on their own (1-atm) run products. The line of Zhang et al. intersects ours at ~1700°C but has a significantly steeper slope and yields diffusivities more than an order of magnitude lower at ~1200°C. The dashed line on Figure 14 shows the temperature dependence of $\tilde{D}$ as determined by application of Wagner's (1969) solution to obtain diffusivities from our own 2.5-GPa experiments. This line nearly coincides with the one resulting from the simplified method described in the preceding paragraph—the lines are in fact indistinguishable given the significant uncertainty in the fit to the interdiffusion coefficients obtained by the Wagner method. Our method is neither as rigorous nor as general as that of Wagner (1969), but it is much

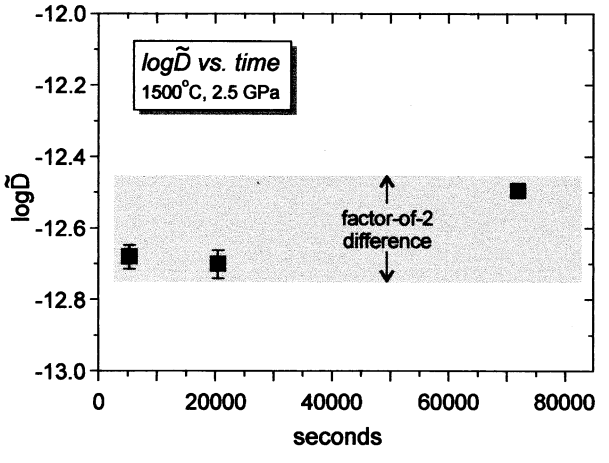

Fig. 15. Mg-Al interdiffusion coefficient vs. time for three experiments at 1500°C and 2.5 GPa.

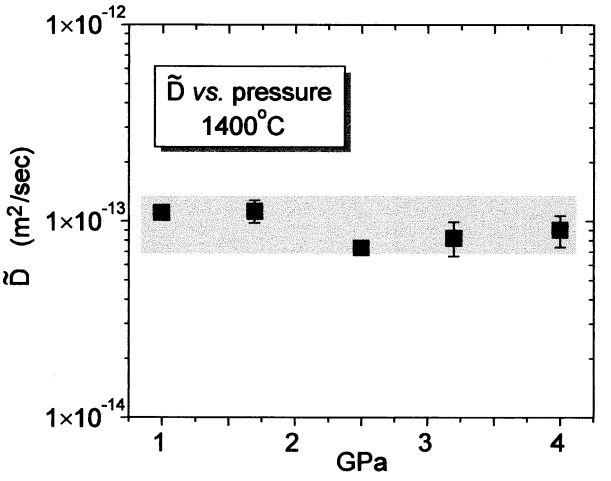

Fig. 16. Mg-Al interdiffusion coefficient vs. pressure at 1400°C.

easier to implement, inasmuch as the Wagner solution requires analytical curve-fitting or numerical integration of the concentration gradients. Our approach is a practical alternative for obtaining interdiffusion coefficients by analysis of reaction product layers in cases where the exchange mechanism is understood and the gradients in the reaction product are linear. Moreover, Eqn. 15 reveals a relatively simple relationship between the quantity that is easily measured in "layer-growth" experiments (i.e., ΔX) and the diffusivity that actually governs the growth rate of the product phase. Although derived in a different way, Eqn. 15 is similar in form to the result of Booth (1948; see also Brady, 1983),

$$D_{\text{eff}} = \frac{\Delta X^2}{2t} \times \frac{\rho_m}{\rho_s}, \tag{16}$$

where D_{eff} is the effective diffusivity of the mobile component in the reaction product layer and ρ refers to the density of the diffusant in the source (ρ_s) and in the layer (ρ_m). Booth's treatment assumes one mobile component and unidirectional growth of the reaction product layer. With adjustments for differences in the physical model, Eqn. 16 yields diffusivities higher by a factor of four than those given by Eqn. 15. The fourfold difference arises because spinel grows in both directions from the original interface, supplied by interdiffusing cations.

It could be concluded from Figure 14 that computation of $\tilde{D}$ destroys the elegant P-T systematics of spinel growth as represented by Figures 4 to 6. It is now clear that the rate of spinel growth is sensitive to changes in pressure not because of an intrinsic effect of pressure on diffusion in spinel (Fig. 16), but because the composition of spinel in equilibrium with corundum changes markedly with pressure (Fig. 9). Indeed, the linear relationship between ln(k) and P (Fig. 6) appears to be due entirely to the pressure dependence of phase relations in the MgO-Al_2O_3 system. This explains the curious shallowing of the slopes in Figure 6 with decreasing temperature. This trend would indicate a positive dependence on temperature of the activation volume for $Mg^{2+} \leftrightarrow Al^{3+}$ interdiffusion if the rate of spinel growth were controlled solely by a pressure-dependent diffusivity. To our knowledge, such a dependence has never been reported.

In comparing $\tilde{D}$ with k, two points are worth reiterating: first, k is much easier to measure accurately (especially at low temperature), and has practical value in systematizing and predicting reaction progress; and second, $\tilde{D}$ is a "purer" quantity in that reflects only the rate of transport through the product layer, whereas k includes components due to both transport rate and chemical potential differences across the layer. The dependencies of k on temperature and pressure do not illuminate any fundamental aspects of the reaction kinetics (i.e., activation energy and activation volume for diffusion). The activation energy for $Mg^{2+} \leftrightarrow Al^{3+}$ interdiffusion (234 kJ/mol) is almost a factor of two lower than the apparent activation energy for spinel growth as represented by the temperature dependence of k.

A final question remains concerning the nature of $Mg^{2+} \leftrightarrow Al^{3+}$ interdiffusion: What is the diffusion pathway? Do Al^{3+} and Mg^{2+} ions diffuse along grain boundaries or through the crystal? It has been implicitly assumed to this point that the flux of ions across the growing spinel layer takes place through the spinel lattice. The arguments for lattice-diffusion control are circumstantial. First, the EMP data suggest no intragrain heterogeneity, so lattice diffusion is apparently effective at the scale of individual spinel grains. Because the spinel grain size is of the same order as the overall thickness of the polycrystalline spinel layer (Fig. 12), lattice diffusion appears capable of effective Mg^{2+} and Al^{3+} transport at length scale of the layer. Another key observation is that, like the polycrystalline periclase and corundum in our experiments, the spinel coarsens with time. In a grain boundary-controlled diffusion regime, coarsening should lead to a time-dependent k and $\tilde{D}$ (because coarsening eliminates grain boundaries), yet these quantities are demonstrably independent of time. The sum total of circumstantial evidence for control of spinel growth by lattice diffusion of Mg^{2+} and Al^{3+} thus appears reasonably strong. However, the possibility that compositional anomalies and rate-controlling fluxes occur at grain boundaries cannot be ruled out. The 234 kJ/mol activation energy seems reasonable for lattice diffusion of relatively small ions through an oxide structure (see compilations by Freer, 1981, and by Brady, 1995; see specifically Freer and Hauptman, 1978), but it is not definitive either. Our activation energy is lower than the 384 kJ/mol of Sheng et al. (1992) for Mg self-diffusion in spinel, and our diffusivities are significantly higher over most of the temperature range of our study (the Arrhenius lines cross at ~2000°C, but the maximum temperature of actual data in the Sheng et al., 1992, study is 1553°C). The discrepancy between the self-diffusion and interdiffusion data could be interpreted to mean that there exists a grain-boundary contribution to the interdiffusion coefficients reported here, or it could be due to the significant vacancy population in the spinels grown by reaction of MgO with Al_2O_3 (see section 3.2.2). If spinel growth in our study is indeed controlled by lattice diffusion, the lack of pressure dependence of $\tilde{D}$ (Fig. 16) is intriguing. Our results may indicate that cation diffusion in close-packed oxide structures is relatively immune to lithosphere-scale changes in pressure because of the high bulk modulus of the lattice (Finger et al., 1986). Alternatively, we may simply have shown that grain-boundary diffusion is insensitive to changes in pressure.

This section on diffusion would be incomplete without some comment on the possibility that oxygen diffusion plays a role in spinel growth. As detailed above, our model and the data on which it is based do not require mobile oxygen. However, our analytical method would detect only a substantial net flux of oxygen, and even then only indirectly. By use of SIMS analysis of an experimental run product similar to ours, J. A. Van Orman (personal communication) confirmed that interdiffusion of oxygen isotopes does occur. At 2000°C and 15 GPa, a ~100-μm-long $^{18}O/^{16}O$ interdiffusion profile developed across the periclase/spinel/corundum contact region. The spinel layer formed during the run was ~20 μm thick, suggesting that the rate of oxygen self-diffusion may be comparable with that of Mg $\leftrightarrow$ Al interdiffusion in spinel at these conditions. This possibility seems inconsistent with the collective database on self-diffusion in spinel (for oxygen: Reddy and Cooper, 1981; Ando and Oishi, 1983; Ryerson and McKeegan, 1994; for magnesium, Sheng et al., 1992), which indicates higher diffusivities for Mg than for O. However, the nonstoichiometry of our spinels may affect the relative diffusivities (Reddy and Cooper, 1981). In addition, none of the previous studies addresses Al diffusion, which may be rate-limiting to the overall process of spinel growth. Given all the evidence, it seems likely that oxygen was mobile in our experiments, although its mobility is not required for spinel growth. This may explain the behavior of the Pt foil marker: if Mg, Al, and O are all mobile in the system, then the position of an inert marker may be determined by interfacial energy considerations rather than by atom fluxes—that is, the Pt may simply tend to move with the migrating periclase/spinel interphase boundary.

4. CONCLUSION

The results of this study corroborate and extend earlier efforts by materials scientists in demonstrating highly systematic temperature and time dependence of the spinel-forming reaction $MgO + Al_2O_3 \rightarrow MgAl_2O_4$. Different experimental strategies and a more comprehensive data set have allowed us to deduce with reasonable certainty the details of spinel growth at the expense of corundum and periclase (these reactants are consumed in a 3:1 ratio). A principal new conclusion is that the rate of spinel growth is markedly slowed by pressure increases achievable within the Earth's lithosphere. This sensitivity to pressure arises not because the rate-controlling diffusion process— interdiffusion of Mg^{2+} and Al^{3+} ions across the newly formed spinel layer—is pressure dependent, but because elevated pressure suppresses the stoichiometric flexibility of $MgAl_2O_4$.

There exist few, if any, instances where the reaction between corundum and periclase has direct geologic relevance. Accordingly, the usefulness to geoscientists of our data and the resulting model may be mainly heuristic. Our simple, practical technique for extracting component diffusivities should be applicable to other systems in which the chemical potential gradients across the product layer are reflected in linear or monotonic compositional variations of interdiffusing elements. We hope the model will constitute a useful interpretational framework for the study of other "armoring" reactions observed both in the laboratory and in natural rocks. The general approach taken here might prove effective for extracting cation diffusivities in cases where other methods are impractical or unworkable. The direct application of our results to mapping temperature in solid-media pressure assemblies almost certainly will

be useful to other experimenters; this subject is discussed in a companion article published elsewhere (Watson et al., 2002).

Acknowledgments—We thank David Wark for help with various aspects of the EMP work and the acquisition of high-contrast BSE images. Jim Van Orman and Bob Doremus provided invaluable comments on the manuscript, as did John Brady and one other anonymous official reviewer. Conversations with Jim Van Orman, John Brady, and Frank Spear forced us to strengthen the case for control spinel growth kinetics by Mg-Al interdiffusion. This work was supported by the National Science Foundation (grant EAR-9804794).

*Associate editor:*M. S. Ghiorso

REFERENCES

Alper A. M., McNally R. N., Ribbe P. H., and Doman R. C. (1962) The system MgO-$MgAl_2O_4$. *J. Am. Ceram. Soc.* **45,** 263–268.

Ando K. and Oishi Y. (1983) Effect of ratio of surface area to volume on oxygen self-diffusion coefficients determined for crushed MgO-Al_2O_3 spinels. *J. Am. Ceram. Soc.* **66,** C131–C132.

Ashworth J. R. and Sheplev V. S. (1997) Diffusion modeling of metamorphic layered coronas with stability criterion and consideration of affinity. *Geochim. Cosmochim. Acta* **61,** 3671–3689.

Booth F. (1948) A note on the theory of surface diffusion reactions. *Trans. Faraday Soc.* **44,** 796–801.

Boyd F. R. and England J. L. (1960) Apparatus for phase equilibrium measurements at pressures up to 50 kb and temperatures up to 1750°C. *J. Geophys. Res.* **65,** 741–748.

Brady J. B. (1983) Intergranular diffusion in metamorphic rocks. *Am. J. Sci.* **283A,** 181–200.

Brady J. B. (1995) Diffusion data for silicate minerals, glasses, and liquids. In *Mineral Physics and Crystallography: A Handbook of Physical Constants* (ed. T. J. Ahrens), pp. 269–290. American Geophysical Union.

Carlson W. D. and Johnson C. D. (1991) Coronal reaction textures in garnet amphibolites of the Llano Uplift. *Am. Mineral.* **76,** 756–772.

Carter R. E. (1961) Mechanism of solid-state reaction between magnesium oxide and aluminum oxide and between magnesium oxide and ferric oxide. *J. Am. Ceram. Soc.* **44,** 116–120.

Finger L. W., Hazen R. M., and Hofmeister A. (1986) High-pressure crystal chemistry of spinel ($MgAl_2O_4$) and magnetite: Comparisons with silicate spinels. *Phys. Chem. Minerals.* **13,** 215–220.

Freer R. (1981) Diffusion n silicate minerals and glasses: A data digest and guide to the literature. *Contrib. Mineral. Petrol.* **76,** 440–454.

Freer R. and Hauptman Z. (1978) An experimental study of magnetite–titanomagnetite interdiffusion. *Phys. Earth Planet. Int.* **16,** 223–231.

Joesten R. (1977) Evolution of mineral assemblage zoning in diffusion metasomatism. *Geochim. Cosmochim. Acta* **41,** 649–670.

Johnson C. D. and Carlson W. D. (1990) The origin of olivine-plagioclase coronas in metagabbros from the Adirondack Mountains, New York. *J. Metam. Geol.* **8,** 697–717.

Li D. X., Piroux P., Heuer A. H., Yadavalli S., and Flynn C. P. (1992) A high-resolution electron microscopy study of MgO/Al_2O_3 interfaces and $MgAl_2O_4$ spinel formation. *Phil. Mag. A* **65,** 403–425.

MacKenzie K. J. D. and Ryan M. J. (1981) Effect of electric fields on solid-state reactions between oxides. *J. Mater. Sci.* **16,** 579–588.

Mao H. K. and Bell P. M. (1971) Behavior of thermocouples in the single-stage piston-cylinder apparatus. *Carnegie Inst. Wash. Yearbook* **69,** 207–216.

Navias L. (1961) Preparation and properties of spinel made by vapor transport and diffusion in the system MgO-Al_2O_3. *J. Am. Ceram. Soc.* **44,** 434–436.

Reddy K. P. R. and Cooper A. R. (1981) Oxygen diffusion in magnesium aluminate spinel. *J. Am. Ceram. Soc.* **64,** 368–371.

Robie R. A., Hemingway B. S., and Fisher J. R. (1978) *Thermodynamic Properties of Minerals and Related Substances at 298.15K and 1 bar (10^5 pascals) Pressure and Higher Temperatures.* Bulletin 1452. U.S. Geological Survey.

Rossi R. C. and Fulrath R. M. (1963) Epitaxial growth of spinel by reaction in the solid state. *J. Am. Ceram. Soc.* **46,** 145–149.

Ryerson F. J. and McKeegan K. D. (1994) Determination of oxygen self-diffusion in åkermanite, anorthite, diopside, and spinel: Implications for oxygen isotopic anomalies and the thermal histories of Ca-Al–rich inclusions. *Geochim. Cosmochim. Acta* **58,** 3713–3734.

Sheng Y. J., Wasserburg G. J., and Hutcheon I. D. (1992) Self-diffusion of Mg in spinel and in equilibrium melts: Constraints on flash heating of silicates. *Geochim. Cosmochim. Acta* **56,** 2535–2546.

Tammann G. (1920) Über Anlauffarben von metallen. *Zeitschr. Anorganische Allgemeine Chem.* **111,** 78–99.

Ting C-J and Lu H-Y. (1999) Defect reactions and the controlling mechanism in the sintering of magnesium aluminate spinel. *J. Am. Ceram. Soc.* **82,** 841–848.

Wagner C. (1969) The evaluation of data obtained with diffusion couples of binary single-phase and multiphase systems. *Acta Metall.* **17,** 99–107.

Watson E. B., Wark D. A., Price J. D and Van Orman J. A. (2002) Mapping the thermal structure of solid-media pressure assemblies. *Contrib. Mineral. Petrol.* **142,** 640–652.

Whitney W. P. II and Stubican V. S. (1971a) Interdiffusion studies in the system MgO-Al_2O_3. *J. Phys. Chem. Solids* **32,** 305–312.

Whitney W. P. II and Stubican V. S. (1971b) Interdiffusion in the system MgO-$MgAl_2O_4$. *J. Am. Ceram. Soc.* **54,** 349–352.

Yamaguchi G. and Tokuda T. (1967) Some aspects of solid state reactions between oxides. *Bull. Chem. Soc. Jpn.* **40,** 843–851.

Zhang P., DebRoy T., and Seetharaman S. (1996) Interdiffusion in the MgO-Al_2O_3 spinel with or without some dopants. *Metall. Mat. Trans. A* **27A,** 2105–2114.